PAPER

Check for updates

Circularly polarized activity from two photon excitable europium and samarium chiral bioprobes†

Silvia Mizzoni,[ab] Silvia Ruggieri, [ID][a] Annika Sickinger,[b] François Riobé, [ID][b] Laure Guy,[b] Margaux Roux,[b] Guillaume Micouin,[b] Akos Banyasz, [ID][b] Olivier Maury, [ID][*b] Bruno Baguenard,[c] Amina Bensalah-Ledoux,[c] Stéphan Guy,[c] Alexei Grichine,[d] Xuan-Nhi Nguyen,[e] Andrea Cimarelli,[e] Martina Sanadar,[f] Andrea Melchior[*f] and Fabio Piccinelli [ID][*a]

In this contribution, two couples of cationic enantiomeric complexes [(*R*,*R*)-[Ln**L**]Cl and (*S*,*S*)-[Ln**L**]Cl, with Ln = Sm and Eu and **L** = *N*,*N*′-bis(2-pyridylmethyl)-1,2-(*R*,*R* or *S*,*S*)-cyclohexanediamine functionalized at sp³ N with the picolinate *antennae* **2**] have been synthesized and spectroscopically characterized in polar protic solvents, such as water and methanol. The good sensitization of Sm(III) and Eu(III) luminescence by the picolinate *antenna* is documented, upon both a one photon absorption process (at about 330 nm) and a two photon absorption process (at 720 nm). The complexes exhibit good CPL activity, in particular for the magnetic dipole (MD) allowed transitions, which are the $^4G_{5/2} \rightarrow {}^6H_{5/2}$ (564 nm) of Sm(III) and the $^5D_0 \rightarrow {}^7F_1$ (593 nm) of Eu(III). Both complexes are highly stable in aqueous solution (log K = 20.13 for the Eu**L** species chosen as the representative) and only one main species is present at physiological pH (7.4). Among the three possible isomeric complexes, DFT calculations on the Y(III) counterpart reveal the highest stability of the C_1-symmetric *cis*−O, O−N, N isomer, in agreement with the presence of only one Eu(III) emitting species in solution. Furthermore, one solvent molecule is bound to the metal ions, giving rise to 9-fold coordinated complexes. Preliminary biphotonic imaging experiments on the (*S*,*S*)-[Eu**L**]Cl complex reveal that it can be easily internalized in two different cell lines (namely 293T cancer cells and THP-1 macrophages) with perinuclear diffuse localisation in the cytosol. Both Sm(III) and Eu(III) complexes can be considered promising candidates as NIR-to-RED *in cellulo* chiroptical bioprobes and a possible extension to the *in vivo* experiment will be further investigated.

[a] *Luminescent Materials Laboratory, DB, Università di Verona, and INSTM, UdR Verona, Strada Le Grazie 15, 37134 Verona, Italy. E-mail: fabio.piccinelli@univr.it*

[b] *Univ Lyon, ENS de Lyon, CNRS UMR 5182, Laboratoire de Chimie, Lyon F-69342, France. E-mail: olivier.maury@ens-lyon.fr*

[c] *Univ. Lyon, Institut Lumière Matière, UMR 5306 CNRS–Université Claude Bernard, 10 rue Ada Byron, Lyon 1, F-69622 Villeurbanne Cedex, France*

[d] *Institute for Advanced Biosciences, University Grenoble Alpes, Inserm U1209, CNRS, UMR 5309, Site Santé, Allée des Alpes, 38700, La Tronche, France*

[e] *Centre International de Recherche en Infectiologie (CIRI), Univ Lyon, Inserm, U1111, Université Claude Bernard Lyon 1, CNRS, UMR5308, ENS de Lyon, Lyon, France*

[f] *Dipartimento Politecnico di Ingegneria e Architettura, Laboratorio di Tecnologie Chimiche, Università di Udine, via Cotonificio 108, 33100 Udine, Italy. E-mail: andrea.melchior@uniud.it*

† Electronic supplementary information (ESI) available: ¹H-NMR, HR-MS, and FT-IR spectra of **3**; potentiometric titration, and DFT calculations of the **L**; HR-MS, FT-IR, electronic absorption, excitation, emission, luminescence decay curves of all the complexes; quantum yield measurements, ECD spectra, CPL spectra of Sm(III) and Eu(III) complexes; photostability test of complex (*S*,*S*)-[Eu**L**]Cl; emission spectra upon two-photon excitation of Eu(III) complexes. The photophysical measurements have been performed in water and/or methanol. See DOI: https://doi.org/10.1039/d2tc05362d

Introduction

To date, luminescent metal complexes based on trivalent lanthanide ions have been broadly employed as optical probes for imaging[1–4] and luminescence sensing.[5–14] For these kinds of biological applications, a high value of brightness (*B*) is required. $B = \varepsilon \cdot \phi_{ovl} = \varepsilon \cdot \eta_{sens} \cdot \phi_{int}$, where ε is the molar absorption coefficient, ϕ_{ovl} is the overall quantum yield, *i.e.*, the ratio of emitted/absorbed photons by the lanthanide complex, η_{sens} is the overall energy transfer efficiency and ϕ_{int} is the intrinsic quantum yield, *i.e.* the ratio of emitted/absorbed photons upon direct excitation into a luminescent level of the lanthanide ion. Within the complex, the use of chromophoric ligands can ensure high ε and η_{sens} values, since they are capable, at the same time, of strong absorption of light (high ε value) and efficiently transfer the excitation energy to the lanthanide ion (high η_{sens} values). On the other hand, to guarantee high ϕ_{int} values nonradiative processes should be avoided, since

4188 | *J. Mater. Chem. C*, 2023, **11**, 4188–4202

This journal is © The Royal Society of Chemistry 2023

they negatively impact the intrinsic quantum yield. Among these processes, the multiphonon relaxation (MPR) is notable; it is particularly effective when high energy vibrational modes (*e.g.* C–H, N–H, and O–H stretching), close to the luminescent lanthanide ion, couple with its electronic levels.[15–17] The presence of solvents, possessing these vibrations, around the metal ion (*i.e.* water) can be avoided upon binding the lanthanide ion to a polydentate organic ligand, which occupies all the possible coordination sites of the metal cation. Apart from designing a suitable chromophoric ligand capable of protecting from the aqueous medium the lanthanide ion and sensitizing its luminescence, one additional important task is to ensure a suitable excitation wavelength to the system. Often, UV light, which is not optimal for experiments involving living cells and organisms, is employed to excite the heteroaromatic chromophore. In addition, the very small depth of penetration in tissues of the UV light prevents its use in *in vivo* tests. An elegant solution to overcome this problem is represented by using NIR light as an excitation source, which is harmless for the cells and at the same time penetrates deep into the skin and biological tissues. NIR excitation is commonly used in the case of luminescent lanthanide complexes sensitized by two–photon (2P) excitable ligands.[18–25] Two–photon absorption (TPA) is a nonlinear optical (NLO) phenomenon[26] which adds crucial advantages for biological application, such as excitation (in the NIR region) with confocal character, giving rise to 3D resolution. These characteristics are combined with the unique photophysical properties of lanthanide ions [*i.e.*, sharp emission bands with large pseudo-Stokes shifts ranging from the visible region to the near-infrared (NIR) region and long lifetimes enabling time-delayed detection] in complexes with two photon absorption properties. Furthermore, still in the biological context, like for example microscopy and bioassays, another interesting optical property of lanthanide complexes, such as circularly polarized luminescence (CPL), has proved very useful.[13,27,28] The coupling of CPL activity with non-linear excitation in a single molecule or in inorganic compounds has been reported for a few examples in the literature,[29–33] although it can open new avenues in the design, fabrication and application of optical materials in the field of bioimaging. To date, to the best of our knowledge, only one example has been reported on the combination of CPL activity stimulated by TPA involving a lanthanide-based complex.[34] This contribution paves the way for the investigation of chiral molecular interactions in living cells using mild NIR excitation. The CPL signal detected by means of a suitable experimental system allows us to determine the different localization within the cells of the couple of Eu(III)-based enantiomeric complexes.

In our contribution, the synthesis and a full optical and chiroptical spectroscopic characterization of two enantiomeric Eu(III)- and Sm(III)-based complexes (Fig. 1) are presented. These molecules exhibit good CPL activity in the orange-red visible spectral region and their metal-centered luminescence can be sensitized by efficient TPA excitation of the ligand around 700 nm. The Eu(III) complex is easily internalized within two different cell lines, displaying its characteristic red
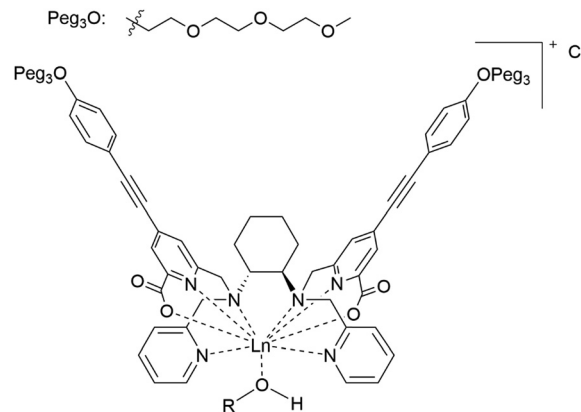

Fig. 1 (*R*,*R*)-[Ln**L**]Cl complexes discussed in this contribution [with Ln = Eu(III), Gd(III) and Sm(III)]; ROH = solvent molecule (H_2O or CH_3OH). Also (*S*,*S*) enantiomers are considered in this work.

emission upon NIR excitation. These investigated complexes represent new examples of TPA-based CPL chiral bioprobes for emerging chiroptical applications in the field of bioimaging.

Experimental section

General

Unless stated otherwise, all reactions of air- and/or water-sensitive compounds were carried out under an inert gas atmosphere using standard Schlenk techniques. Solvents were purchased from Fisher Scientific, VWR Chemicals or Carlo Erba Reagents and used without further purification. All the solvents used for the synthesis were stored over 3 Å molecular sieves. $CDCl_3$ was supplied by Eurisotop. Starting materials were purchased from Sigma-Aldrich, TCI, Alfa Aesar or Acros Organics. Column chromatography was performed using silica gel (40–63 μm) from VWR Chemicals. [1]H, ^{13}C and the corresponding two-dimensional nuclear magnetic resonance (NMR) spectra were recorded at room temperature on a Bruker Avance III 300 or on a Bruker Ascend 400 spectrometer. The chemical shifts in ppm were referenced to the solvent residual proton signals ($CDCl_3$: 7.26 ppm). The multiplicities of the signals were abbreviated as follows: s (singlet), d (doublet), t (triplet), q (quartet), quint (quintet), dd (doublet of doublets), m (multiplet) and br (broad signal). IR Spectra were recorded on a Spectrum 65, 100 and 400 series FT-IR spectrometer. Typical 32 scans were accumulated for each spectrum (resolution of 4 cm^{-1}). High resolution mass spectrometry measurements (HR-MS) were performed at the Centre Commun de Spectrometrie de Masse (Villeurbanne, France) with a MicroOTOFQ II (Bruker) using electrospray ionization (ESI).

Both the enantiomers of *N*,*N*′-bis(2-pyridylmethyl)-1,2-(*R*,*R* or *S*,*S*)-cyclohexanediamine molecule **1** and the mesylated picolinate antennas **2** (Fig. 2), have been synthesized respectively as reported in the literature.[23,35] $EuCl_3 \cdot 6H_2O$, $SmCl_3 \cdot 6H_2O$ and $GdCl_3 \cdot 6H_2O$ (Aldrich, 98%) have been stored under vacuum for several days at 80 °C and then transferred into a glove box.

This journal is © The Royal Society of Chemistry 2023

J. Mater. Chem. C, 2023, **11**, 4188–4202 | **4189**

Synthesis of 3 and [LnL]Cl complexes

The synthesis of molecule **3** is reported in Fig. 2. In particular, a suspension of compound **1** (0.099 g, 0.33 mmol, 1 equiv., both enantiomers (R,R) and (S,S) were used) and K_2CO_3 (0.184 g, 1.33 mmol, 4 equiv.) in acetonitrile (5 mL) were mixed vigorously for 15 min under an inert atmosphere at room temperature. A solution of compound **2** (0.339 g, 0.68 mmol, 2 equiv.) in acetonitrile (3 mL) was added to the previous mixture and the resulting mixture was refluxed at 85 °C for 24 h under an inert atmosphere. After cooling the solution to room temperature, the mixture was filtered from salts and solvent evaporated under vacuum. The crude product was purified on a Silica column using a dichloromethane/methanol (92/8 V/V, Rf 0.24) mixture as the eluent yielding compound (S,S)-**3** (0.170 g, 0.15 mmol, yield = 45%) [(R,R)-**3** (0.172 g, 0.15 mmol, 46%)] as a brown oil.

(S,S)-**3** ^{1}H NMR (300 MHz, CDCl$_3$) reported in Fig. S1 (ESI†): δ 8.43 (br s, 2H), 7.85 (br, 3H), 7.50 (br s, 2H), 7.34 (d, 6H), 6.97 (m, 2H), 6.87 (d, 5H), 4.17 (m, 4H), 3.91 (m, 11 H), 3.75(m, 18H), 3.55 (m, 4 H), 3.38 (s, 6H), 2.88 (br s, 1H) 2.35 (br s, 2H), 1.83 (br s, 2H), 1.18 (m, 5H).

(R,R)-**3** ^{1}H NMR (300 MHz, CDCl$_3$) reported in Fig. S2 (ESI†): δ 8.40 (br s, 2H), 7.83 (br, 4H), 7.46 (br s, 2H), 7.39 (d, 6H), 6.99 (m, 2H), 6.88 (d, 4H), 4.17 (m, 4H), 3.90 (m, 13H), 3.66 (m, 14

H), 3.55 (m, 5H), 3.38 (s, 6H), 2.34 (br s, 2H), 1.90 (br s, 2H), 1.17 (m, 6H).

ESI-HR-MS (positive, CH$_3$CN; m/z) calcd for $[C_{64}H_{74}N_6O_{12}]^+$: 1119.5437, found: 1119.5429 (S,S)-**3**, 1119.5438 (R,R)-**3**, $[M + H]^+$; calcd for $[C_{64}H_{74}N_6NaO_{12}]^+$: 1141.5257, found: 1141.5249 (S,S)-**3**, 1141.5256 (R,R)-**3**, $[M + Na]^+$. See Fig. S3 and S4 (ESI†).

FT-IR (cm^{-1}, ATR) reported in Fig. S5 (ESI†): C=O: 1725; C≡C: 2206.

The synthesis of the complexes, depicted in Fig. 2, was performed as follows. A solution of compound **3** (R,R) or (S,S) (0.020 g, 0.018 mmol, 1 equiv.) in MeOH (11 mL) and a solution of sodium hydroxide (0.162 mL, 0.162 mmol, 9 equiv.) in water (1 M) were mixed together and stirred overnight. Then the solution was acidified until pH = 5.5 using HCl (0.1 M) and the Ln(III) chloride salt (EuCl$_3$·6H$_2$O 0.0086 g, SmCl$_3$·6H$_2$O 0.0085 g and GdCl$_3$·6H$_2$O 0.0086 g; 0.023 mmol, 1.3 equiv.) was added to the solution and left stirring overnight. Then the reaction mixture was concentrated, the residue dissolved in dichloromethane washed with water to remove salts in excess; then it was dried by Na$_2$SO$_4$. All the complexes were obtained as pale-yellow solids.

(S,S)-[Eu**L**]Cl: 0.020 g (yield 91%); (R,R)-[Eu**L**]Cl: 0.021 g (yield 93%).

ESI-HR-MS (positive, CH$_3$CN; m/z) calcd for $[C_{62}H_{68}EuN_6O_{12}]^+$: 1241.4135, found: 1241.4116 (S,S)-[Eu**L**]Cl, 1241.4116 (R,R)-[Eu**L**]Cl, $[M]^+$. See Fig. S8 and S9 (ESI†).

FT-IR (cm^{-1}, ATR) reported in Fig. S10 (ESI†): C=O: 1634; C≡C: 2206.

(S,S)-[Sm**L**]Cl: 0.021 g (Yield 95%); (R,R)-[Sm**L**]Cl: 0.022 g (Yield 98%).

ESI-HR-MS (positive, CH$_3$CN; m/z) calcd for $[C_{62}H_{68}SmN_6O_{12}]^+$: 1240.4047, found: 1240.4087 (S,S)-[Sm**L**]Cl, 1240.4091 (R,R)-[Sm**L**]Cl, $[M]^+$. See Fig. S11 and S12 (ESI†).

FT-IR (cm^{-1}, ATR) reported in Fig. S13 (ESI†): C=O: 1634; C≡C: 2206.

(S,S)-[Gd**L**]Cl: 0.010 g (yield 45%).

ESI-HR-MS (positive, CH$_3$CN; m/z) calcd for $[C_{62}H_{68}GdN_6O_{12}]^+$: 1246.4326, found: 1246.4121, $[M]^+$. See Fig. S14 (ESI†).

FT-IR (cm^{-1}, ATR) reported in Fig. S15 (ESI†): C=O: 1634; C≡C: 2206.

Potentiometric and spectrophotometric titrations

Stock solutions of NaOH and HCl were prepared using Fixanal 0.1 mol dm^{-3} (Fluka Analytical) standard solution and ultrapure water (>18 MΩ cm) from a MilliQ system (ELGA Purelab UHQ). The ionic strength of all solutions was adjusted to 0.1 mol dm^{-3} with NaCl (Riedel–de Häen). Stock solutions of Eu(III) (80 mM) were prepared by dissolving the chloride hexahydrate salts (SigmaAldrich) and standardized by titration with EDTA and xylenol orange as the indicator in acetate buffer.[36] Protonation constants of the ligand were determined by acid–base potentiometric titrations. Electromotive force (emf) data were collected by using a computer-controlled potentiometer (Amel Instruments, 338 pH Meter) connected to a combined glass electrode (Metrohm Unitrode 6.0259.100). The electrode was calibrated before each lecture by an
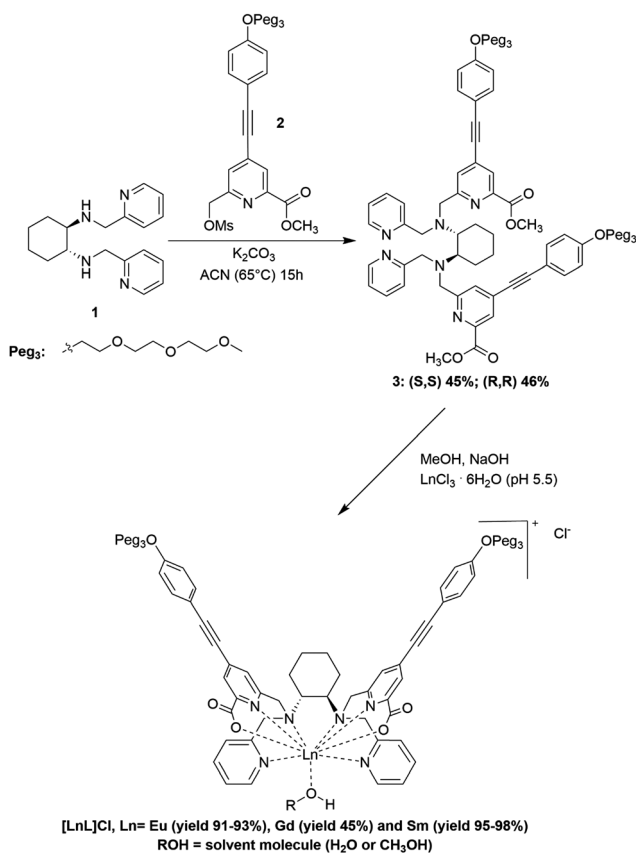

Fig. 2 Synthetic pathway for the synthesis of [Ln**L**]Cl complex. The (R,R) enantiomer of the ligand is reported but the synthesis was performed also with the (S,S) one, in the case of Eu(III) and Sm(III) complexes.

acid–base titration with standard HCl and NaOH solutions. The content of carbonate in solution, as well as free acid concentrations in stock metal ions solutions, was determined by Gran's method.[37] Titrations were performed by adding NaOH 0.1 mol dm^{-3} to ligand solutions (typical concentration $\sim$0.4 mM) by a computer-controlled burette (Metrohm Dosimat 765). About 150 data points were collected and processed by means of the Hyperquad[38] program to obtain the protonation constants.

Complex formation constants were determined by combined potentiometric/UV–vis titrations.[39] Absorption spectra were collected with a Varian Cary 50 spectrophotometer equipped with an optical fiber probe (1 cm optical path length) which was inserted into the titration cell which contained a solution with the ligand (total concentration = 0.016 mM) and an equimolar quantity of Eu(III).

In all cases, the titration cells were maintained at constant temperature (25 °C) with a circulatory bath and under Ar radial flux to avoid carbonate contamination. Absorbance data at multiple wavelengths were analyzed using the HypSpec program[40] to obtain the complex formation constants.

DFT calculations

All minimum energy structures of the complexes were obtained by means of DFT calculations run in Gaussian 16 (version A.03).[41] The ωB97X–D functional[42] was used with the 6–31+G(d) basis set for all ligand atoms and MWB28 pseudopotential and valence electrons basis set[43] for the metal ion as they previously showed good performance in predicting structural parameters and energies of lanthanides[44] and transition metal complexes.[45] The paramagnetic Eu(III) ions have been replaced by Y(III) which is a suitable substitute as shown in previous works[46] and as can be deduced from the isostructural complexes found with the analogous hexa-dentate ligands EDTA and CDTA, which result in being 9–coordinated in the first case ($[LnL(H_2O)_3]^-$) and 8–coordinated in the second ($[LnL(H_2O)_2]^-$).[47–49] To reduce the computational cost of the geometry searches, the PEGylated chain of L has been replaced by a methyl ether group (–OCH$_3$) to give the simplified ligand L'. Geometry optimizations were carried out including solvent (water) effects by means of the polarizable continuum model (PCM).[50]

Photophysical measurements

Absorption spectra were recorded on a JASCO V–650 spectrophotometer in diluted solution (ca. 10^{-5} or 10^{-6} mol L^{-1}), using spectrophotometric grade solvents. Emission spectra were measured using a Horiba–Jobin–Yvon Fluorolog-3 fluorimeter. The steady–state luminescence was excited by unpolarized light from a 450 W xenon continuous wave (CW) lamp and detected at an angle of 90° for measurements of dilute solutions (10 mm quartz cuvette) either by using a Hamamatsu R928 photomultiplier tube. Spectra were corrected for both excitation source light–intensity variation and emission spectral responses. Lanthanides(III) luminescence and phosphorescence lifetimes (τ) were obtained by pulsed excitation with a FL-1040 UP

xenon lamp. Luminescence decay curves were fitted using the mono-exponential equation:

$$I(t) = I_0 \times e^{-\frac{t}{\tau}}$$

Overall luminescence quantum yields were measured for the complexes by using secondary methods described in the literature.[51] Diluted solutions with an absorbance lower than 0.1 were used and the following equation was employed:

$$\frac{\phi_{ovl(x)}}{\phi_{ovl(r)}} = \left[\frac{A_r(\lambda)}{A_x(\lambda)}\right] \times \left[\frac{n_x^2}{n_r^2}\right] \times \left[\frac{D_x}{D_r}\right]$$

Where A is the absorbance at the excitation wavelength λ, n is the refractive index and D is the integrated luminescence intensity. "r" and "x" stand for reference and sample, respectively. The reference is quinine bisulfate in a 1 N aqueous solution of sulfuric acid ($\phi_{ovl(r)} = 0.546$). Excitations of reference and sample compounds were performed at the same wavelength. In practice, the absorbance and spectra of a minimum of 5 solutions at different optical densities were considered (see Fig. S24 (ESI†), for Eu(III) complexes and Fig. S25 (ESI†), for Sm(III) complexes). The emission area was then plotted as a function of the optical density for both the compound and the reference. Each slope corresponds to the ratio $\phi_{ovl(x/r)}/n^2_{x/r}$ in the equation above and is directly linked to the compound quantum yield.

Lifetime was calculated from luminescence decay measurements, carried out at least 4 times by changing slits opening.

Chiroptical measurements

Measurements of circular dichroism in the UV/Vis region were performed on a JASCO J-710 spectropolarimeter on complex solutions with concentrations around 10^{-5} to 10^{-6} M.

VIS-CPL spectra are recorded on a homemade apparatus.[52] Solutions (10^{-4} mol L^{-1}) in a quartz cuvette are excited by UV light from a diode (365 nm). The fluorescence is collected with a lens and separated by means of an achromatic $\lambda/4$ waveplate (45°) and a polarizing beam splitter. With this arrangement, the light is split into two components of either left- or right-circularly polarized light. Each arm is further imaged on one side of a fiber bundle. The other extremity of the bundle is focused on the entrance slit of a spectrophotometer. The light spectrally separated is imaged on a CCD camera. The "upper/lower" part of the camera records the left- or right-handed circularly polarized spectra. Because of the brightness of the molecules as well as their high g_{lum}, this set-up allows fast recording of the CPL spectra in less than ten seconds.

Two-photon (2P) spectroscopy

Two-photon excitation spectra and two-photon cross-sections were obtained by two-photon excited fluorescence measurements of diluted methanol solutions of the compounds (10^{-5} mol L^{-1}) using a femtosecond Ti:sapphire laser (Coherent Chameleon Ultra II, 80 MHz, 140 fs) in the range 720–990 nm. The excitation beam (2.6 mm diameter) was focused with a 75 mm focal length

This journal is © The Royal Society of Chemistry 2023

J. Mater. Chem. C, 2023, **11**, 4188–4202 | **4191**

lens to the sample. The upconverted fluorescence was collected at right-angles using a 30 mm focal length doublet lens. After filtering the scattered excitation beam by low-pass filters, the florescence was coupled to a fiber optic spectrometer (Avantes Hero). The sample was contained in a 1×1 cm quartz cell and continuously stirred with a magnetic stirrer to avoid thermal effects. After verifying that the fluorescence intensity exhibited quadratic intensity dependence for each sample, the incident power was adjusted to 40 mW. Calibration of the 2P absorption spectra was performed at each excitation wavelength by comparison with that of fluorescein (10^{-5} mol L^{-1}, pH 11) as the reference compound.[53]

Cell analysis

Human embryonic kidney HEK293T cells (ATCC cat. CRL-3216) and monocytic THP-1 cells (ATCC cat. TIB-202) were respectively maintained in complete medium without phenol red DMEM (Gibco, cat A1443001, lot 2323301) and RPMI-1640 (Gibco, cat. 32404014, lot 2448998), supplemented with 10% Fetal Calf Serum (FCS, Sigma cat. F7524) and a mix of penicillin (100 U ml^{-1})/streptomycin (100 µg ml^{-1}) (Gibco, cat 15140122, lot 2441841). THP-1 cells media was also supplemented with 0.05 mM beta-mercaptoethanol (Euromedex, cat. 4227-A) and 10 mM HEPES (Sigma, cat. H0887) and macrophage-like differentiation was induced upon a forty-eight hours treatment with 100 ng ml^{-1} of phorbol 12-myristate 13-acetate (PMA) (Sigma cat. P1585).

Prior to the incubation with the complexes, HEK293T and THP-1 were respectively seeded at 500 000 cells and 1×10^6 cells in a specific 35 mm µ-dish (IBIDI, Dish, cat. 81156) optimized for live imaging. After removing the medium, the cells were incubated with 400 µL of fresh medium with complexes diluted at 10^{-4} M over 6 hours. Before imaging, the culture medium was removed and the cells were rinsed twice with a new culture medium. *Toxicity study*: viability assays were performed at two different time points to test the cytotoxicity of the complexes. HEK293T and THP-1 were incubated with the complexes S or R, as in the conditions used for live imaging analysis. Cells were also treated with etoposide at 50 µM (Sigma-Aldrich; ref E1383) as a positive control of cytotoxicity. After 6 hours of treatment, cells were either immediately analyzed, or washed with PBS and replenished with fresh media for an additional 18 hours. The proportion of live/dead cells was measured after staining with trypan blue (Sigma-Aldrich ref T8154-100 ml) and cell counting.

Confocal and two-photon microscopy

All confocal experiments were performed using a LSM710 NLO (Carl Zeiss) confocal laser scanning microscope based on the inverted motorized stand (AxioObserver, Zeiss). The excitation was provided by a Ti:Sa femtosecond tunable laser (Chameleon, Ultra II, Coherent) for 2P excitation at 700 nm in descanned detection mode. 5% laser power was used. The pinhole was close to 1.4 Airy Unit. The objective used is Zeiss 63× (oil) Plan-Apochromat. Spectral imaging was realized using an internal Quasar detector in the range 460–730 nm with the resolution around 10 nm. 10% laser power was used in the spectral mode.

Results and discussion

Synthesis

The synthesis of the pro-ligand **3** (*R,R* and *S,S*) was readily achieved upon alkylation of the cyclohexyl-diamine precursor **1** with two equivalents of functionalized dipicolinate antenna **2** in basic media and purified by column chromatography (Fig. 2). The synthesis of the [LnL]Cl complex was performed by a one pot (including two-steps) protocol that involves the hydrolysis of both ester groups of **3**, under basic conditions, followed by complexation at pH = 5.5 of the resulting ligand with the related lanthanide(III) chloride salt (LnCl$_3$·6H$_2$O; with Ln = Eu, Gd and Sm). A pale-yellow solid was obtained in good yield (around 90%) for all the complexes. Both the enantiomers of **3** are considered in the case of Eu and Sm, whilst in the case of the Gd counterpart only the (*S,S*) one was synthesized. As expected, the presence of the PEGylated chains ensures amphiphilic properties to the complexes and the required solubility in organic solvents, water, and polar protic solvents in general.

Complex formation equilibria

The protonation constants for ligand **L** were obtained from the best fit of pH data and are reported in Table 1, along with those relative to other ligands previously studied by some of us[12,46] or others[54,55] (Fig. 3) for comparison.

Titration curves and speciation plot for acid–base equilibria for ligand **L** are presented in Fig. S6a (ESI†). In addition to the potentiometric study, a spectrophotometric acid–base titration was carried out to evidence the species distribution (Fig. S6b, ESI†) which confirmed the protonation constants obtained from potentiometry. The first protonation constant ($\log K_1 = 9.65$) can be assigned to a tertiary amine, in agreement with those already reported ($\log K \sim 8.6$–10.3, depending on the substituents).[46,58–60] The second protonation ($\log K_2 = 8.88$) can be assigned to the protonation of a chromophore as evidenced by the net variation of absorbance at 320 nm (ε_{320}, Fig. S6b, ESI†) upon formation of the LH$_2$ species. Then the absorbance remains constant until pH 4.5. The $\log K_2$ value is higher than that proposed for 2–picoline ($\log K = 6.14$)[61] and also substituted pyridines (*e.g.* for bis-((2-pyridiyl)methyl)-amine $\log K = 7.3$).[62] This could be due to a stabilization of the LH$_2$ species through intramolecular hydrogen bonds, as proposed in Fig. S7 (ESI†), where the minimum energy structures of possible isomers of LH$_2$ are shown. The energy of the isomers (a) and (b), where one proton is attached to a pyridine and picolinate nitrogen atoms, respectively is nearly the same, differing by less than 0.4 kcal mol^{-1}. On the contrary the protonation of the second amine nitrogen or of the acetate group is less favored as the isomers are 4.7 and 3.5 kcal mol^{-1} higher in energy with respect to the species (a). Therefore, the LH$_2$ could be a mixture of micro-species involving the picolinate and pyridine groups.

4192 | *J. Mater. Chem. C*, 2023, **11**, 4188–4202

This journal is © The Royal Society of Chemistry 2023

Table 1 Protonation constants ($\log K_j$) for **L** and complex formation constants ($\log \beta$) with Eu(III) at 25 °C and μ = 0.1 M NaCl. Additional protonation and formation constant data for comparison with other ligands are also reported. Charges are omitted

Reaction	Ligand L	H$_2$bpcd[46]	PyC3A[12]	H$_4$CHXoctapa[54,55]	H$_4$octapa[56,57]
log K_j					
L + H ⇌ HL	9.65 ± 0.04	9.72	10.26	9.23	8.58
HL + H ⇌ H$_2$L	8.88 ± 0.05	5.87	6.33	5.40	5.43
H$_2$L + H ⇌ H$_3$L	3.60 ± 0.05	2.94	3.67	3.94	3.75
H$_3$L + H ⇌ H$_4$L	2.20 ± 0.10	2.22	2.01	2.24	3.08
H$_4$L + H ⇌ H$_5$L	—	—	—	1.82	2.21
H$_5$L + H ⇌ H$_6$L	—	—	—	1.91	1.61
H$_6$L + H ⇌ H$_7$L	—	—	—	—	0.12
H$_7$L + H ⇌ H$_8$L	—	—	—	—	−0.46
log β					
L + Eu ⇌ EuL	20.13 ± 0.05	11.20	15.68	—	—
EuL + H ⇌ EuLH	4.69 ± 0.06	—	—	—	—
EuLH + H ⇌ EuLH$_2$	2.76 ± 0.05	—	—	—	—
L + Gd ⇌ GdL	—	—	—	19.92	20.23
GdL + H ⇌ GdLH	—	—	—	1.02	—
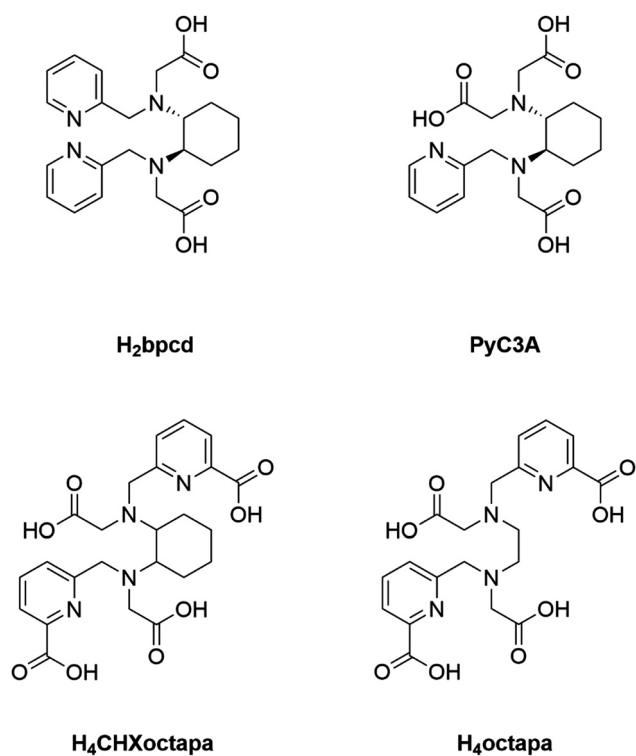
Fig. 3 Structural formulas of a series of hexa- and octadentate ligands similar to **L**.

Below pH 4.5 the absorbance decreases further and then increases again in correspondence to the formation of the LH$_3$ and LH$_4$ species and can be assigned to the carboxylate groups of the picolinate.[46] The last protonation constant ($\log K_4$ = 2.21) is associated with the carboxylate groups of the picolinate in agreement with those already reported ($\log K \sim$ 2.03–3.58, depending on the substituents).[63,64]

The spectrophotometric data relative to the complex formation (Fig. 4a) were best fitted by a speciation model including the formation of three Eu species (EuL, EuLH, EuLH$_2$, Table 1). In Fig. 4b the speciation diagram of the Eu(III) complexes are

shown, also with the molar absorbance at 336 nm (ε_{336}) as a function of pH. The EuL complex starts to form above pH = 4.1 in correspondence with a net increase of ε_{336}. Eu(III) emission spectra recorded in the 5.4–11.3 pH range confirm the presence of a single Eu–containing species. The stability constant obtained for EuL is comparable to those of other Ln(III) complexes with similar acyclic ligands containing picolinate chelating groups,[55] with the formation of an octadentate complex. According to this model, at physiological pH = 7.4 and 1 : 1 Eu : L molar ratio, the ML species is largely prevalent ($\sim$100%) and, in the perspective of *in vitro* application experiments, the stability looks suitable, as it is close to that of macrocyclic ligands already employed in molecular imaging applications (*e.g.* DO3A or DTPA derivatives with $\log \beta$ values in the 18–22 range).[65–67]

The possible structure of the species in solution has been determined by DFT calculations. The complex considered for the structural study was the [**YL′**(H$_2$O)]$^+$, where the polyethylene chains were replaced by methyl groups, in its isomeric form depending on the relative arrangement of the heteroaromatic and acetate groups (*trans*-OO, *trans*-NN and *cis*–OO,NN) with respect to the DACH moiety (Fig. 5). Interestingly, we show that the water molecule is retained in the first coordination sphere of Y(III), thus making it a good model for the corresponding Eu(III) complexes for which the experimental hydration number (q = 1) was found (*vide infra* Table 2). Therefore, the metal here is 9-coordinated differently from what was found for similar complexes previously studied which resulted in being 8-coordinated.[12,46,68] The energy of the isomers *trans*–OO, *trans*-NN did not differ significantly ($<$ 0.1 kcal mol^{-1}) while *cis*-OO,NN is 4.6 kcal mol^{-1} more stable than the others. This finding suggests that in aqueous solutions the latter should be the prevalent one.

Photophysical properties

The photophysical properties of the *S,S*-[Gd**L**]Cl complex have been first investigated in order to determine the energy diagram of the coordinated ligand. At room temperature, the complex presents broad intense absorption and emission bands centered at 336 nm and 450 nm (Fig. 6), respectively assigned to the
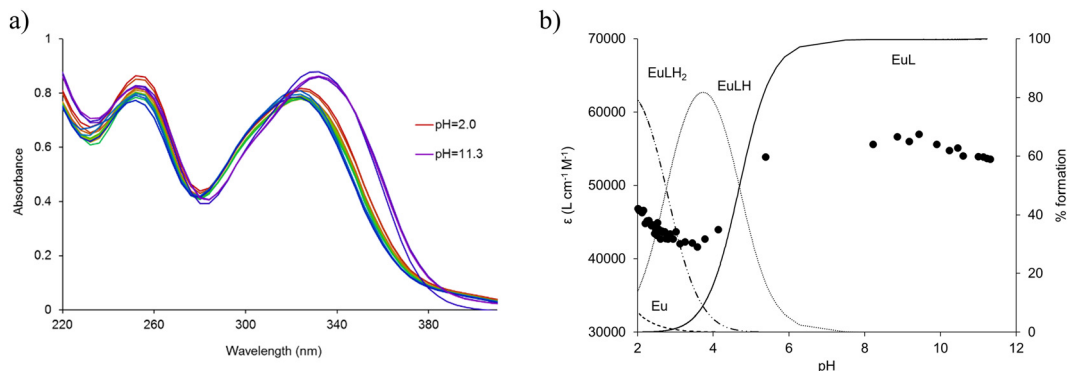
Fig. 4 (a) UV-vis absorption spectra changes during the acid−base titration of the ligand L (0.016 mM) in the presence of an equimolar quantity of Eu(III); (b) changes in the molar absorbance, ε_{336} (●) during the titration and calculated species distribution relative to the total metal in solution. Charges are omitted for clarity.
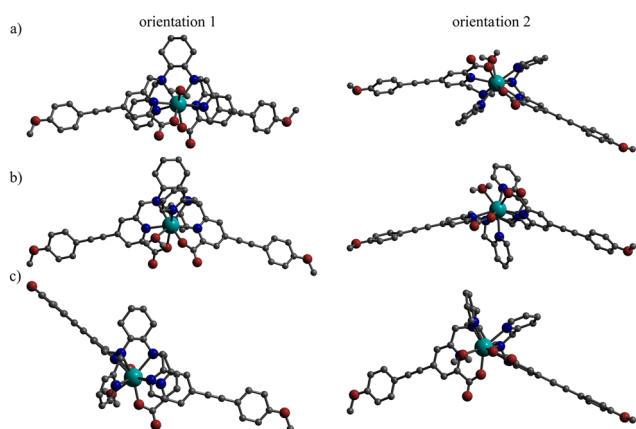

Fig. 5 Minimum energy structures of the possible [YL′H$_2$O] conformational isomers *trans−O,O* (a), *trans−N,N* (b), and *cis−O,O−N,N* (c) along the axis perpendicular to the cyclohexane plane (orientation 1) and though it (orientation 2). Hydrogens bound to carbon atoms have been hidden for clarity.

IntraLigand Charge Transfer (ILCT) transition from the O-donor to the picolinic accepting moieties.[23] The energy level of the relaxed excited ILCT state, E(ILCT*) = 26 500 cm^{-1} was estimated by the tangent method on the emission spectrum. Cooling the ethanol/methanol solution down to 77 K results in the formation of an organic glass and profound modification of the emission spectrum. The fluorescence band is significantly blue-shifted to 387 nm ($\Delta\lambda$ = 63 nm) compared to the room temperature one. This behavior can be rationalized by the fact that, at low temperature in the glassy solid matrix, the suppression of molecular motions avoids solvent reorganization around the excited chromophore, resulting in the increase of charge transfer state energy level.[69] In addition, a weak signal is observed in the red tail of the fluorescence band. It is isolated using time-gated measurement with a delay of 50 μs. The resulting structured emission is therefore characteristic of the long-lived phosphorescence of the associated triplet state (^3T, τ_{obs}= 1.62(1) ms at 77 K, Fig. S16, ESI†) whose energy is determined at $E(^3T)$ = 20 830 ± 80 cm^{-1} (asterisk in Fig. 6). These first measurements

allow us to determine the simplified energy level diagram of the ligand (Fig. S17, ESI†) and a comparison with the energy levels of the accepting Eu(III) and Sm(III) state clearly indicates that the ligand is suitable to act as a sensitizing antenna.

The absorption, emission and chiroptical properties (CD and CPL) of the corresponding Eu(III) and Sm(III) complexes have been measured in diluted water or methanol solutions and all the results are compiled in Table 2 and Table S1 (ESI†), respectively.

First, as already observed,[73] all complexes present very similar absorption spectra whatever the nature of the central metal ion (Eu, Sm) with two strong absorption peaks at 254 nm (ε around 35 000 L mol^{-1} cm^{-1}) and 336 nm (ε around 41 000–45 000 L mol^{-1} cm^{-1}) (Fig. 7). The transition at 245 nm is related to the pyridine ring absorption,[46] whilst as above-mentioned, the broad and structureless band centered at 336 nm is assigned to the ILCT transition. Almost identical conclusions can be drawn when the absorption spectra were collected in methanol (Fig. S18, ESI†).

As clearly illustrated by the excitation spectra in water (Fig. S19, ESI†), irradiation in the ILCT transition induced the yellow-orange emission and red emission of Sm(III)- and Eu(III)-based complexes, respectively. The emission profiles (Fig. 8 in water and Fig. S20 and S21, ESI† in MeOH) are identical for the two enantiomers and are characteristic of the $^5D_0 \rightarrow {}^7F_J$ (J = 0 to 4) transitions for Eu(III) and $^4G_{5/2} \rightarrow {}^5H_J$ (J = 5/2 to 11/2) for Sm(III). The absence of any residual ligand centered emission (or the very weak one observed for Sm) suggests a very efficient sensitization process involving either a direct ILCT mechanism or an indirect pathway mediated by the ligand triplet state (Fig. S17, ESI†).[74]

In the case of Eu(III) the overall quantum yield is found around 10% in water and 22% in methanol (Table 2). These relatively low values can be explained by the analysis of the lifetime measurement. The observed lifetimes in water for Eu(III)-based complexes (reported in Table 2) were calculated from the analysis of the Eu(III) $^5D_0$ luminescence decay curves, (Fig. S22, ESI†). All the curves are appropriately fitted by a single exponential function. The comparison of the lifetimes

4194 | *J. Mater. Chem. C*, 2023, **11**, 4188–4202

This journal is © The Royal Society of Chemistry 2023

Table 2 Photophysical data of europium and samarium complexes in water at room temperature

	(S,S)-[EuL]Cl	(R,R)-[EuL]Cl	(S,S)-[SmL]Cl	(R,R)-[SmL]Cl
ε	44 652 (336 nm)	43 364 (336 nm)	41 678 (336 nm)	41 642 (336 nm)
(L mol^{-1} cm^{-1})	35 465 (254 nm)	31 117 (254 nm)	33 048 (254 nm)	35 258 (254 nm)
τ(μs)	480 (1270 D$_2$O)	520 (1350 D$_2$O)	15 (72 D$_2$O)	14 (66 D$_2$O)
q	1.4[a]	1.3[a]	0.97[b]	1.06[b]
ϕ[c]	0.11	0.10	0.004	0.005
σ[d](GM)	112	86	—	—
g_{abs}	0.00015 (259 nm)	−0.00013 (259 nm)	0.00015 (259 nm)	−0.00010 (259 nm)
	0.00021 (290 nm)	−0.00072 (290 nm)	0.00017 (285 nm)	−0.00019 (285 nm)
g_{lum}[e]	−0.205 (593 nm)	+0.236 (593 nm)	+0.133 (564 nm)	−0.127 (564 nm)
	+0.040 (615 nm)	−0.043 (615 nm)	−0.093 (599 nm)	+0.088 (599 nm)
B$^{336\ nm}$ (L mol^{-1} cm^{-1})	4912	4336	167	208

[a] $q = 1.05(\tau_{H_2O}^{-1} - \tau_{D_2O}^{-1})$.[70,71] [b] $q = 0.0254(\tau_{H_2O}^{-1} - \tau_{D_2O}^{-1}) - 0.37$.[72] [c] Using quinine sulfate in H$_2$SO$_4$ 1N as the standard (Φ = 54.6%, λ_{ex} = 345 nm), error about ±10%. [d] Determined in methanol, error about ±20%. [e] g_{lum} values are referred to the most intense component of the $^5D_0 \to {}^7F_1$ (593 nm) and $^5D_0 \to {}^7F_2$ (615 nm) transitions for Eu^{3+} and $^4G_{5/2} \to {}^6H_{5/2}$ (564 nm) and $^4G_{5/2} \to {}^6H_{7/2}$ (599 nm) transitions for Sm^{3+}.
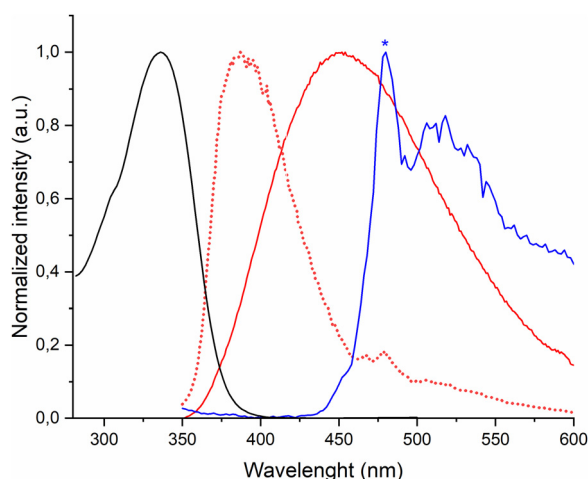

Fig. 6 Normalized absorption (black) and emission of (S,S)-[GdL]Cl in ethanol/methanol 4/1 solution at room temperature (red, solid) and 77 K emission (red, dashed) and phosphorescence spectrum (blue) after application of a 50 μs delay. The asterisk indicates the value of $E(^3T)$. All the emission spectra were collected upon excitation at 336 nm.
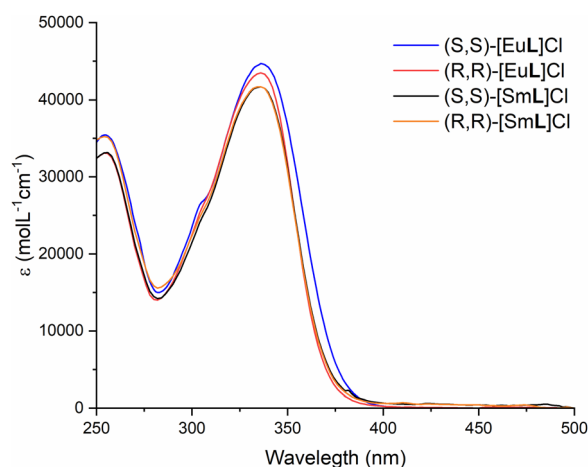

Fig. 7 Absorption spectra of both enantiomers of [EuL]Cl and [SmL]Cl in water at room temperature.

recorded in hydrogenated and deuterated solvents allow us to calculate the number of water (q) and methanol (m) molecules directly coordinated to Eu(III) ions, using the empirical Horrock's equation.[70,71] As q (resp, m) values are close to 1 for both the enantiomers of the complex, we can conclude that one solvent molecule is present in the inner coordination sphere of Eu(III). The presence of OH vibrators in the first coordination sphere is well known to induce a strong luminescence quenching and therefore explain the modest overall quantum yield measured for the complexes.

In addition, europium(III) complexes are particularly sensitive to ligand field effects and careful analysis of the emission band splitting and relative intensity provides interesting information about the symmetry of the [EuL]Cl coordination polyhedron.[75–77] The emission spectrum (Fig. 8) presents the characteristic $^5D_0 \to {}^7F_J$ (J = 0 to 4) transitions of europium(III) where the hypersensitive J = 2 transition remains clearly the most intense. The presence of only one intense emission peak for the $^5D_0 \to {}^7F_0$ transition of Eu(III) calls for the presence of only one emitting species in which the local symmetry of the metal ion shows an axial character.[76] In this context, C_n, C_{nv}, or C_s are the only possible point symmetries in the presence of sizeable intensity of the $^5D_0 \to {}^7F_0$ transition.[78] Because of the chirality of the ligand, the C_s point symmetry can be ruled out and the only remaining symmetries, compatible with the molecular structure are C_1, C_2 or C_{2v}. We can hypothesize that the most stable isomer found by DFT calculation (cis–O,O–N,N; Fig. 5), showing an Eu(III) ion with a C_1 point symmetry, is the dominant species in solution observed by luminescence spectroscopy.

Concerning the Samarium(III) complexes, its $^4G_{5/2}$ emitting state is located at a comparable energy to that of europium(III) (Sm(III) $^4G_{5/2} \sim 18\,000$ cm^{-1}; Eu(III) $^5D_{1/0}$ 19 000 and 17 400 cm^{-1})[79] and can therefore be sensitized by the same ligand. As it is possible to notice from Fig. 8 upon excitation at 336 nm, a weak residual ligand-centred emission is observed accompanied by the characteristic Sm(III) emission profile spreading in the visible region assigned to the $^4G_{5/2} \to {}^6H_J$ (J = 5/2–11/2) transitions with the hypersensitive one, J = 9/2, at 645 nm. The additional emission bands located in the near-infra red have
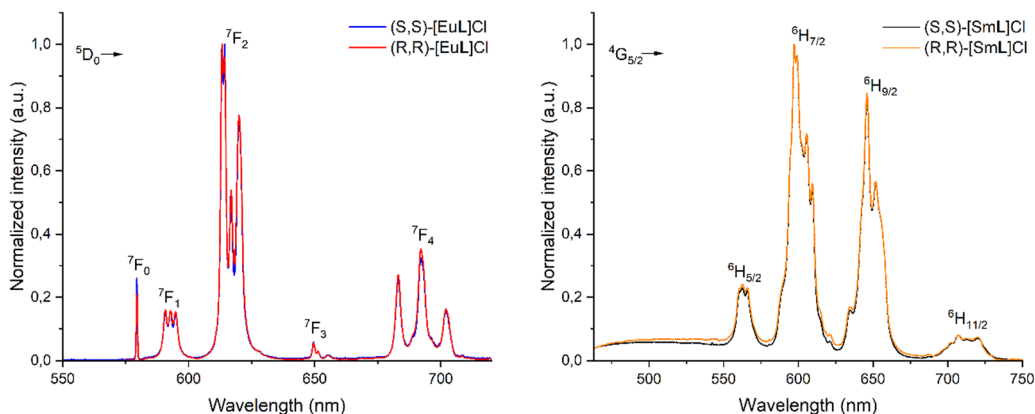
This journal is © The Royal Society of Chemistry 2023

J. Mater. Chem. C, 2023, **11**, 4188–4202 | **4195**

Fig. 8 Luminescence emission spectra of (*S*,*S*)-[Ln**L**]Cl and (*R*,*R*)-[Ln**L**]Cl [Ln = Eu (left), Sm (right)] complexes in water emitting in the visible region. Excitation at 336 nm.

not been observed in this case, because of lower detector sensitivity in this region. The overall quantum yield (ca 0.5% in water and 2% in MeOH) is weaker than the Eu(III) counterpart. Indeed, Sm(III) suffers from an intrinsic disadvantage of having a weaker luminescence intensity because of a smaller energy gap between the emitting state and the next lower energy level: $\Delta E(^{4}G_{5/2} \rightarrow {}^{6}F_{11/2})$ of *ca.* 7500 cm^{-1} of Sm(III) *versus* $\Delta E(^{5}D_{0} \rightarrow {}^{7}F_{6})$ of *ca.* 12 500 cm^{-1} of Eu(III) resulting in enhanced non-radiative deactivation processes from X–H vibrators (X= O, N but also C).[80,81]

In addition, as for the Eu(III) counterpart, the [Sm**L**]Cl complex is expected to present a similar coordination environment characterized by the presence of one water (or methanol) molecule in the inner coordination sphere of the metal ion. Compared to the [Eu**L**]Cl complexes, the differences between water (methanol) and deuterated water (methanol) lifetime values are quite high (Table 2 and S1, ESI†).

This, as before, can be related to the smaller energy gap between the lowest luminescent excited state and the highest ground state. Therefore, lower overtones of the high-energy vibrational modes can match the energy gap of [Sm**L**]Cl, resulting in more efficient quenching of the luminescent state.[82] As expected, based on these lifetimes (see Fig. S23, ESI†) and by using the equation reported in the ref. 72 we calculated a q number around 1 for both the enantiomers of the [Sm**L**]Cl complex in both water and methanol (see Table 2).

The photostability of complex (*S*,*S*)-[Eu**L**]Cl in methanol was also estimated. It is quite good as it amounts to ca 80% after 8 h irradiation (λ_{ex} = 324 nm, P_{inc} = 3,5 mW) under continuous stirring (Fig. S26, ESI†).

Chiroptical spectroscopy

As for the UV–visible electronic absorption, the ECD spectra of the complexes [Eu**L**]Cl and [Sm**L**]Cl in water (Fig. 9) are independent of the nature metal ion (Sm or Eu) and the solvent (water or methanol; compare Fig. 9 and Fig. S27, ESI†). This finding agrees with the ligand-centred nature of the involved electronic transitions. The transition at 250 nm is related to the pyridine ring absorption,[46] whilst as above-mentioned, the

broad band extended at higher wavelengths is assigned to the ILCT transition. It is clear from the spectra that these two transitions are sensitive to the chirality of the structures.

The luminescence of all complexes made them available for circularly polarized luminescence studies. The CPL spectra were recorded in aqueous solution (Fig. 10) and in methanol (Fig. S28, ESI†) at room temperature for both Eu(III)- and Sm(III)-based complexes, upon excitation at 365 nm. The spectra are very well resolved and as expected, the opposite enantiomers display perfect mirror image CPL signatures. The g_{lum} values of the most intense signals are reported in Table 2 and Table S1 (ESI†). As already observed, the f–f transitions featuring a magnetic dipole (MD) character (ΔJ = 0, ± 1 (except $0 \leftrightarrow 0$)) present the highest dissymmetry factor.[83] As frequently observed in the literature,[84] this is the case of the $^{5}D_{0} \rightarrow {}^{7}F_{1}$ transition of [Eu**L**]Cl with a g_{lum}(593 nm) = |0.22|. This is also observed in the MD-allowed Sm(III) transitions like the $^{4}G_{5/2} \rightarrow {}^{6}H_{7/2}$ with g_{lum}(599 nm) = |0.091| and the $^{4}G_{5/2} \rightarrow {}^{6}H_{5/2}$ with g_{lum}(564 nm) = |0.130|. It is worth noting that samarium CPL is less frequent than the europium one (especially in water).[81,85,86] The recorded g_{lum} values of the [Eu**L**]Cl are in line with the ones recorded for similar Eu(III) DACH-based chiral complexes.[46,87,88] On the other hand, it is remarkable the very good g_{lum} values of the [Sm**L**]Cl complex dissolved in methanol (|0.194|, Table S1, ESI†), which is the highest ever recorded for similar Sm(III) complexes containing the DACH chiral ring,[87,88] in general,[46,87] and they are far lower than the record dissymmetry factor values above unity.[89,90]

Although the emission spectra of Eu(III) and Sm(III) complexes in water are almost superimposable to the ones recorded in methanol (see Fig. S29, ESI†), the different CPL signatures of both Eu(III) and Sm(III) complexes when dissolved in these two different solvents are noteworthy. In general, even though for each transition the CPL sign of the different crystal field components does not change with the solvent employed, the pattern recorded in methanol looks more complex. This behaviour can find a possible explanation taking into account the effect of the inner sphere solvent coordination or the overall solvation as recently discussed by D. Parker *et al.*[91] Similarly, in
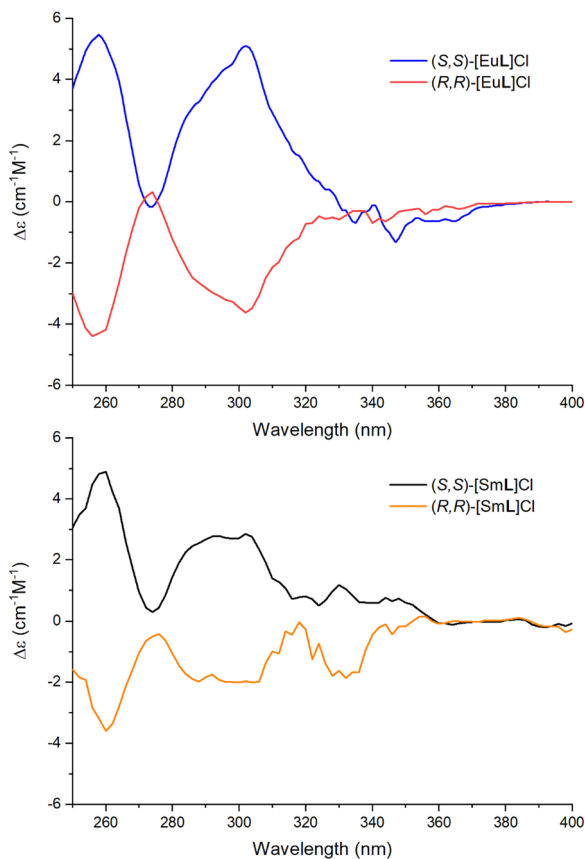
Fig. 9 ECD spectra of both the enantiomers of the [EuL]Cl (up) and [SmL]Cl (bottom) complexes in water (10^{-6} M) at room temperature.

addition to the solvent, other achiral entities can affect the CPL activity of the Ln(III), such as the counterion[87] and the matrix hosting the complex.[92]

Two-photon absorption properties

The two-photon absorption cross-section in the NIR spectral region (700–850 nm) for the (S,S)-[EuL]Cl and (R,R)-[EuL]Cl complexes were measured in methanol using a two-photon excited fluorescence (TPEF) method (Fig. 11). Upon excitation at 720 nm, the characteristic europium(III) emission is obtained (Fig. 11 and Fig. S30, ESI†) and displays a quadratic variation of intensity with respect to the incident laser power, the signature of a 2P-antenna effect (Fig. S31, ESI†).[93] As expected for a non-centrosymmetric compound, the 2P absorption spectrum (Fig. 11) matches very well with the wavelength-doubled one-photon absorption, indicating that the low energy ILCT transition responsible for the europium(III) sensitization is one- and two-photon allowed. Because of the spectral restriction of the laser source the maximum of the 2P cross section is not achieved, and only the red tail of the 2P spectrum can be measured. At 700 nm, the 2P cross-section of both enantiomers is very similar within the uncertainty error of the experimental measurements (112 GM for (S,S)-[EuL]Cl and 86 GM for (R,R)-[EuL]Cl). These values are in the same range as that of other complexes featuring similar antenna chromophores.[23,93–95]
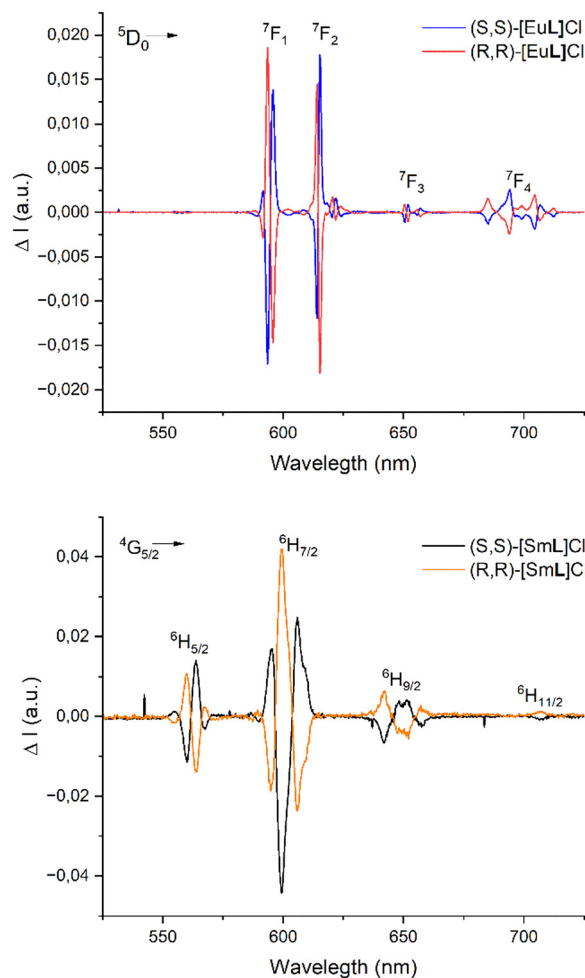

Fig. 10 CPL spectra of (S,S)-[LnL]Cl and (R,R)-[LnL]Cl [Ln = Eu (up), Sm (bottom)] complexes in water emitting in the visible region (λ_{exc} = 365 nm).

(Right) Overlap between the luminescence spectra of (S,S)-[EuL]Cl in methanol at room temperature excited by a one photon process (blue line λ_{exc} = 337 nm) and by a two-photon process (blue dashed λ_{exc} = 720 nm), the lower resolution of the two-photon emission spectrum is due to the larger slit aperture used in the experimental set-up to optimize the signal over noise ratio.

Confocal and two-photon microscopy

The (S,S)-[EuL]Cl complex was then involved in preliminary biphotonic imaging experiments using two different cell lines, namely HEK293T and THP-1 cells that represent adherent neuronal and macrophage precursor cells. The cells were incubated over 6 h with the complex dissolved directly in the culture medium ($c = 10^{-4}$ M). After rinsing, the cells are imaged using 2P-microscopy (λ_{ex} = 700 nm, Fig. 12). For the two cell lines an intense luminescence signal (broad band collection) is collected from the cells suggesting internalization of the complex. The use of the spectral mode of the 2P-microscope allows the emission spectrum in each pixel to be measured enabling us to analyse the different emitting species contribution
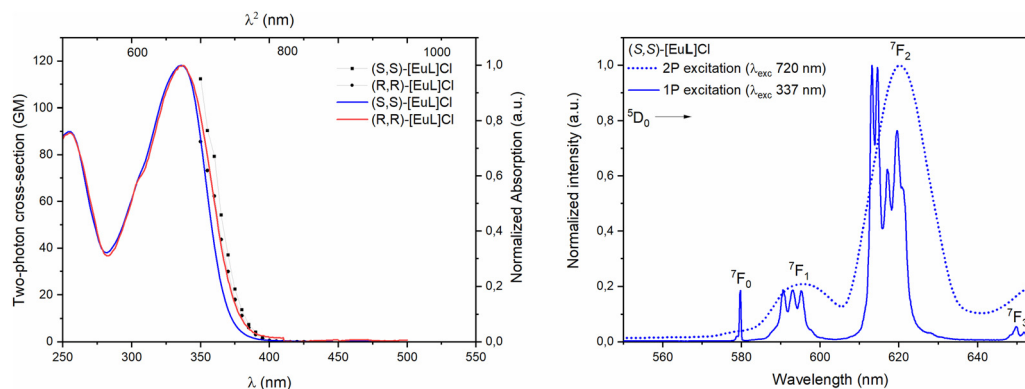
This journal is © The Royal Society of Chemistry 2023

J. Mater. Chem. C, 2023, **11**, 4188–4202 | **4197**

Fig. 11 (left) Normalized absorption spectrum of (*S,S*)-[Eu**L**]Cl and (*R,R*)-[Eu**L**]Cl in MeOH at RT (blue and red line, lower abscissa). Superimposed on this plot is the 2P absorption measured by the TPEF method in methanol in a wavelength doubled scale (■ and ●, upper abscissa).
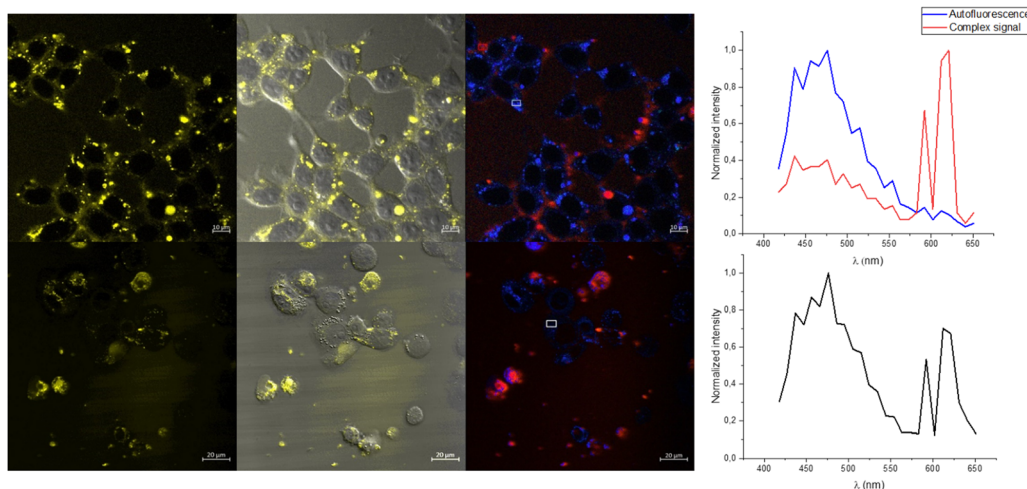

Fig. 12 2P-microscopy imaging of living HEK293T (up) and THP-1 (bottom) cells stained with (*S,S*)-[Eu**L**]Cl (λ_{ex} = 700 nm). (From left to right) Fluorescence images (false colour), overlay of the fluorescence and the transmission (DIC) images, fluorescence images using the spectral mode (real color) and details of the emission spectra recorded in the indicated localization. Panels present the typical results obtained.

inside the cells. Interestingly, this image indicates that the overall luminescence signal is in fact the addition of at least two components: a blue one corresponding to a luminescence signal centred at 470 nm that probably includes the auto-fluorescence of intra-cellular organelles located in the cytoplasm (*e.g.* auto-fluorescence of NAD(P)H located in the mitochondria)[96] and a second contribution, more diffuse and less intense that represents the expected Eu(III) spectral signature. The use of the spectra mode of the microscope is the only method able to decipher between these two different contributions. Indeed, even though the emission maxima of these components are well separated, their relative intensities differ a lot between pixels. Without spectral unmixing, the wide spectral contribution of the strong blue component in the red channel could lead to misinterpretation of the Ln accumulation.

In the present case, thanks to the red component localisation, it is possible to conclude that the (*S,S*)-[Eu**L**]Cl is able to spontaneously internalize in the two different living cell lines. It is important to mention that the (*S,S*)-[Eu**L**]Cl is dissociated in water and is therefore cationic; it has already been

demonstrated that cationic complexes can be internalized *via* an active endocytosis mechanism resulting in a final localisation of the probes in the endosomes and lysosomes, which are small lipidic membrane vesicles located in the cytoplasm,[97,98] but also *via* passive diffusion mechanisms, leading to electrostatic accumulation near the charged inner mitochondria membrane.[99] In the present case, the perinuclear diffuse localisation in the cytosol suggests either a different internalization process, intracellular release of the probe from the endosomes to the cytosol, or their fusion with the endoplasmic reticulum. Further studies are necessary to determine more details of this pathway.

Cytotoxicity

The toxicity of the complexes has been evaluated on the two cell lines studied (HEK293T and THP-1). Neither of the enantiomeric europium complexes exerted a detectable effect on cell viability at the time of the assay (6 h), although a small effect could be noted during prolonged incubation with compound (*R,R*)-[Eu**L**]Cl after 24 h (Fig. 13).
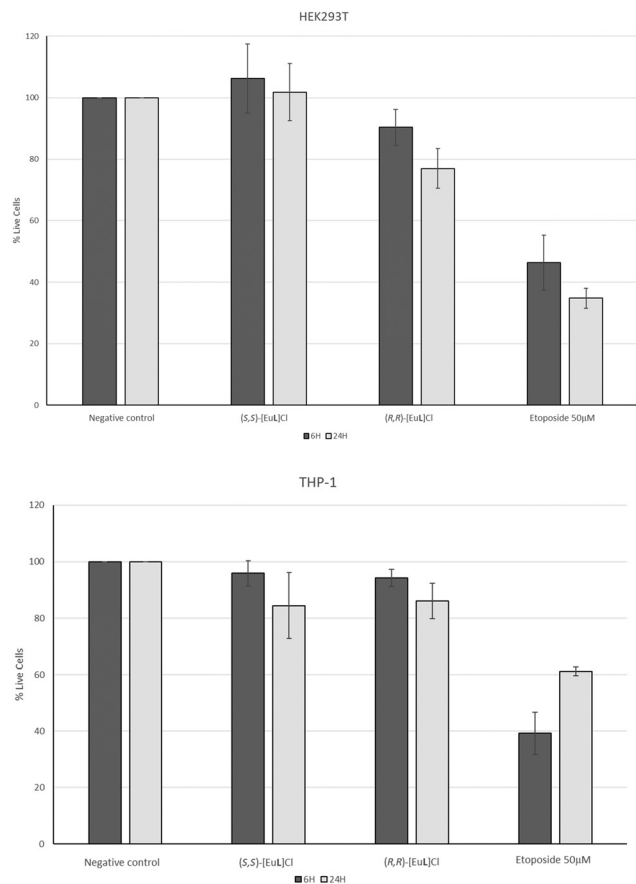
Fig. 13 Cell viability was measured by a trypan blue exclusion assay at the indicated time points on HEK293T (up) and THP-1 (bottom). The graph presents normalized averages and SEM from three and two independent experiments (6 and 24 hours, respectively). Etoposide was used as a positive control of cell death.

Conclusions

At physiological pH, one prevalent cationic, enantiopure, water soluble and highly stable species of $[LnL(H_2O)]^+$ formula (Ln = Sm or Eu) exhibits good CPL activity in correspondence with MD allowed transitions $[^4G_{5/2} \rightarrow {}^6H_{5/2}$ (564 nm) for Sm(III) and $^5D_0 \rightarrow {}^7F_1$ (593 nm) for Eu(III)]. For both Ln(III) ions, CPL is efficiently sensitized upon the absorption of one photon or two photons (at 337 nm) by the extended π-conjugated picolinate *antenna* possessing ILCT and T1 excited states. Similarly, in the case of aqueous solution, when the complexes are dissolved in methanol, one solvent molecule is bound to the metal ion and the photophysical data are similar in the two different solvents. According to the spectroscopic study, DFT calculations on the Y(III) counterpart suggest the presence of one main isomeric complex in solution (the *cis–O,O–N,N* species) in which one water molecule is bound to the metal ion. Preliminary spectroscopic experiments in a complex matrix, where the luminescence and the decay kinetics of the Eu(III) emitting level in the $[EuL(H_2O)]^+$ complex were monitored upon the addition of interfering species, such as BSA (Bovine Serum Albumin), L-lactate, citrate and HCO_3^-, reveal that the coordination

environment of the metal ion remains unchanged and the water molecule is not displaced. This experimental evidence paves the way for the use of these complexes as chiroptical probes in imaging experiments. The applicability of these NIR-to-RED probes has been tested in biphotonic imaging experiments on the enantiopure (*S,S*)-[EuL]Cl complex. This molecule is internalized in two different cell lines (namely 293T cancer cells and THP-1 macrophages) showing almost negligible cytotoxicity. The typical Eu(III) luminescence, triggered upon excitation at 700 nm, suggests perinuclear diffuse localisation of the probe in the cytosol. Further experiments, also using CPL spectroscopy, will be devoted to investigating possible different localizations within the cells of the couple of [EuL]Cl enantiomers. The extension to *in vivo* experiments of these complexes will also be further developed.

Author contributions

Conflicts of interest

There are no conflicts to declare.

Acknowledgements

References

1 K.-L. Wong, J.-C. G. Bünzli and P. A. Tanner, *J. Lumin.*, 2020, **224**, 117256.
2 J.-C. C. G. Bünzli and C. Piguet, *Taking advantage of luminescent lanthanide ions*, Royal Society of Chemistry, 2005, vol. 34.

3 I. Hemmilä, V. Laitala, I. Hemmila and V. Laitala, *J. Fluoresc.*, 2005, **15**, 529–542.

4 E. J. New, D. Parker, D. G. Smith and J. W. Walton, *Curr. Opin. Chem. Biol.*, 2010, **14**, 238–246.

5 H. Tsukube and S. Shinoda, *Chem. Rev.*, 2002, **102**, 2389–2404.

6 Z. Liu, W. He and Z. Guo, *Chem. Soc. Rev.*, 2013, **42**, 1568–1600.

7 F. Piccinelli, M. Leonzio, M. Bettinelli, M. Monari, C. Grazioli, A. Melchior and M. Tolazzi, *Dalton Trans.*, 2016, **45**, 3310–3318.

8 F. Piccinelli, M. Leonzio, M. Bettinelli, A. Melchior, G. Faura and M. Tolazzi, *Inorg. Chim. Acta*, 2016, **453**, 751–756.

9 F. Piccinelli, A. Melchior, A. Speghini, M. Monari, M. Tolazzi and M. Bettinelli, *Polyhedron*, 2013, **57**, 30–38.

10 C. De Rosa, A. Melchior, M. Sanadar, M. Tolazzi, A. Duerkop and F. Piccinelli, *Dalton Trans.*, 2021, **50**, 4700–4712.

11 C. De Rosa, A. Melchior, M. Sanadar, M. Tolazzi, A. Giorgetti, R. P. Ribeiro, C. Nardon and F. Piccinelli, *Inorg. Chem.*, 2020, **59**, 12564–12577.

12 F. Piccinelli, C. De Rosa, A. Melchior, G. Faura, M. Tolazzi and M. Bettinelli, *Dalton Trans.*, 2019, **48**, 1202–1216.

13 M. Leonzio, A. Melchior, G. Faura, M. Tolazzi, M. Bettinelli, F. Zinna, L. Arrico, L. Di Bari and F. Piccinelli, *New J. Chem.*, 2018, **42**, 7931–7939.

14 J. F. C. B. Ramalho, A. N. Carneiro Neto, L. D. Carlos, P. S. André and R. A. S. Ferreira, in *Handbook on the Physics and Chemistry of Rare Earths*, ed. J.-C. G. Bünzli and V. K. Pecharsky, Elsevier, 2022, vol. 61, pp. 31–128.

15 M. J. Weber, *Phys. Rev.*, 1968, **171**, 283–291.

16 J. M. F. Van Dijk and M. F. H. Schuurmans, *J. Chem. Phys.*, 1983, **78**, 5317–5323.

17 H. U. Güdel and M. Pollnau, *J. Alloys Compd.*, 2000, **303–304**, 307–315.

18 A. D'Aléo, A. Picot, P. L. Baldeck, C. Andraud and O. Maury, *Inorg. Chem.*, 2008, **47**, 10269–10279.

19 L.-M. Fu, X.-F. Wen, X.-C. Ai, Y. Sun, Y.-S. Wu, J.-P. Zhang and Y. Wang, *Angew. Chem., Int. Ed.*, 2005, **44**, 747–750.

20 M. H. V. Werts, N. Nerambourg, D. Pélégry, Y. Le Grand and M. Blanchard-Desce, *Photochem. Photobiol. Sci.*, 2005, **4**, 531–538.

21 N. Hamon, A. Roux, M. Beyler, J.-C. Mulatier, C. Andraud, C. Nguyen, M. Maynadier, N. Bettache, A. Duperray, A. Grichine, S. Brasselet, M. Gary-Bobo, O. Maury and R. Tripier, *J. Am. Chem. Soc.*, 2020, **142**, 10184–10197.

22 A. D'Aléo, A. Bourdolle, S. Brustlein, T. Fauquier, A. Grichine, A. Duperray, P. L. Baldeck, C. Andraud, S. Brasselet and O. Maury, *Angew. Chem., Int. Ed.*, 2012, **51**, 6622–6625.

23 M. Soulié, F. Latzko, E. Bourrier, V. Placide, S. J. Butler, R. Pal, J. W. Walton, P. L. Baldeck, B. Le Guennic, C. Andraud, J. M. Zwier, L. Lamarque, D. Parker, O. Maury, B. Le Guennic, C. Andraud, J. M. Zwier, L. Lamarque, D. Parker and O. Maury, *Chem. – Eur. J.*, 2014, **20**, 8636–8646.

24 A. Bourdolle, M. Allali, J.-C. Mulatier, B. Le Guennic, J. M. Zwier, P. L. Baldeck, J.-C. G. Bünzli, C. Andraud, L. Lamarque and O. Maury, *Inorg. Chem.*, 2011, **50**, 4987–4999.

25 A. Bourdolle, M. Allali, A. D'Aléo, P. L. Baldeck, K. Kamada, J. A. G. Williams, H. Le Bozec, C. Andraud and O. Maury, *ChemPhysChem*, 2013, **14**, 3361–3367.

26 C. Andraud and O. Maury, *Eur. J. Inorg. Chem.*, 2009, 4357–4371.

27 J. Yuasa, T. Ohno, H. Tsumatori, R. Shiba, H. Kamikubo, M. Kataoka, Y. Hasegawa and T. Kawai, *Chem. Commun.*, 2013, **49**, 4604–4606.

28 S. Orsini, F. Zinna, T. Biver, L. Di Bari and I. Bonaduce, *RSC Adv.*, 2016, **6**, 96176–96181.

29 S. Míguez-Lago, I. F. A. Mariz, M. A. Medel, J. M. Cuerva, E. Maçôas, C. M. Cruz and A. G. Campaña, *Chem. Sci.*, 2022, **13**, 10267–10272.

30 W. Chen, S. Zhang, M. Zhou, T. Zhao, X. Qin, X. Liu, M. Liu and P. Duan, *J. Phys. Chem. Lett.*, 2019, **10**, 3290–3295.

31 W.-T. Deng, H. Qu, Z.-Y. Huang, L. Shi, Z.-Y. Tang, X.-Y. Cao and J. Tao, *Chem. Commun.*, 2019, **55**, 2210–2213.

32 C. M. Cruz, I. R. Márquez, I. F. A. Mariz, V. Blanco, C. Sánchez-Sánchez, J. M. Sobrado, J. A. Martín-Gago, J. M. Cuerva, E. Maçôas and A. G. Campaña, *Chem. Sci.*, 2018, **9**, 3917–3924.

33 P. Reine, A. M. Ortuño, I. F. A. Mariz, M. Ribagorda, J. M. Cuerva, A. G. Campaña, E. Maçôas and D. Miguel, *Front. Chem.*, 2020, **8**, 306.

34 P. Stachelek, L. MacKenzie, D. Parker and R. Pal, *Nat. Commun.*, 2022, **13**, 553.

35 F. Piccinelli, A. Speghini, M. Monari and M. Bettinelli, *Inorg. Chim. Acta*, 2012, **385**, 65–72.

36 A. I. Vogel and J. Mendham, *Vogel's textbook of quantitative chemical analysis*, Prentice Hall, Harlow, 2000.

37 G. Gran, *Analyst*, 1952, **77**, 661–670.

38 L. Alderighi, P. Gans, A. Ienco, D. Peters, A. Sabatini and A. Vacca, *Coord. Chem. Rev.*, 1999, **184**, 311–318.

39 F. Endrizzi, P. Di Bernardo, P. L. Zanonato, F. Tisato, M. Porchia, A. A. Isse, A. Melchior and M. Tolazzi, *Dalton Trans.*, 2017, **46**, 1455–1466.

40 P. Gans, A. Sabatini and A. Vacca, *Talanta*, 1996, **43**, 1739–1753.

41 M. J. Frisch, G. W. Trucks, H. B. Schlegel, G. E. Scuseria, M. A. Robb, J. R. Cheeseman, G. Scalmani, V. Barone, G. A. Petersson, H. Nakatsuji, X. Li, M. Caricato, A. V. Marenich, J. Bloino, B. G. Janesko, R. Gomperts, B. Mennucci, H. P. Hratchian, J. V. Ortiz, A. F. Izmaylov, J. L. Sonnenberg, D. Williams-Young, F. Ding, F. Lipparini, F. Egidi, J. Goings, B. Peng, A. Petrone, T. Henderson, D. Ranasinghe, V. G. Zakrzewski, J. Gao, N. Rega, G. Zheng, W. Liang, M. Hada, M. Ehara, K. Toyota, R. Fukuda, J. Hasegawa, M. Ishida, T. Nakajima, Y. Honda, O. Kitao, H. Nakai, T. Vreven, K. Throssell, J. Montgomery, Jr., J. E. Peralta, F. Ogliaro, M. J. Bearpark, J. J. Heyd, E. N. Brothers, K. N. Kudin, V. N. Staroverov, T. A. Keith, R. Kobayashi, J. Normand, K. Raghavachari, A. P. Rendell, J. C. Burant, S. S. Iyengar, J. Tomasi, M. Cossi, J. M. Millam, M. Klene, C. Adamo, R. Cammi, J. W. Ochterski, R. L. Martin, K. Morokuma, O. Farkas, J. B. Foresman and D. J. Fox, *Gaussian 16 Rev. A03*, Wallingford, CT, 2016.

4200 | *J. Mater. Chem. C*, 2023, **11**, 4188–4202

This journal is © The Royal Society of Chemistry 2023

42 J. Da Chai and M. Head-Gordon, *Phys. Chem. Chem. Phys.*, 2008, **10**, 6615–6620.

43 D. Andrae, U. Häussermann, M. Dolg, H. Stoll and H. Preuss, *Theor. Chim. Acta*, 1990, **77**, 123–141.

44 A. Roca-Sabio, M. Regueiro-Figueroa, D. Esteban-Gómez, A. de Blas, T. Rodríguez-Blas and C. Platas-Iglesias, *Comput. Theor. Chem.*, 2012, **999**, 93–104.

45 D. Veclani, A. Melchior, M. Tolazzi and J. P. Cerón-Carrasco, *J. Am. Chem. Soc.*, 2018, **140**, 14024–14027.

46 M. Leonzio, A. Melchior, G. Faura, M. Tolazzi, F. Zinna, L. Di Bari and F. Piccinelli, *Inorg. Chem.*, 2017, **56**, 4413–4422.

47 J. Wang, Y. Wang, Z. H. Zhang, X. D. Zhang, J. Tong, X. Z. Liu, X. Y. Liu, Y. Zhang and Z. J. Pan, *J. Struct. Chem.*, 2005, **46**, 895–905.

48 A. Mondry and R. Janicki, *Dalton Trans.*, 2006, 4702–4710.

49 J. Wang, P. Hu, B. Liu, R. Xu, X. Wang, D. Wang, L. Q. Zhang and X. D. Zhang, *J. Struct. Chem.*, 2011, **52**, 568.

50 J. Tomasi, B. Mennucci and R. Cammi, *Chem. Rev.*, 2005, **105**, 2999–3094.

51 D. F. Eaton, *Pure Appl. Chem.*, 1988, **60**, 1107–1114.

52 B. Baguenard, A. Bensalah-Ledoux, L. Guy, F. Riobé, O. Maury and S. Guy, *Nat. Commun.*, 2023, **14**, 1065.

53 S. de Reguardati, J. Pahapill, A. Mikhailov, Y. Stepanenko and A. Rebane, *Opt. Express*, 2016, **24**, 9053–9066.

54 C. F. Ramogida, J. F. Cawthray, E. Boros, C. L. Ferreira, B. O. Patrick, M. J. Adam and C. Orvig, *Inorg. Chem.*, 2015, **54**, 2017–2031.

55 F. Lucio-Martínez, Z. Garda, B. Váradi, F. K. Kálmán, D. Esteban-Gómez, É. Tóth, G. Tircsó and C. Platas-Iglesias, *Inorg. Chem.*, 2022, **61**, 5157–5171.

56 M. de, G. Jaraquemada-Peláez, X. Wang, T. J. Clough, Y. Cao, N. Choudhary, K. Emler, B. O. Patrick and C. Orvig, *Dalton Trans.*, 2017, **46**, 14647–14658.

57 F. K. Kálmán, A. Végh, M. Regueiro-Figueroa, É. Tóth, C. Platas-Iglesias and G. Tircsó, *Inorg. Chem.*, 2015, **54**, 2345–2356.

58 G. Nizou, E. Molnár, N. Hamon, F. K. Kálmán, O. Fougère, O. Rousseaux, D. Esteban-Gòmez, C. Platas-Iglesias, M. Beyler, G. Tircsó and R. Tripier, *Inorg. Chem.*, 2021, **60**, 2390–2405.

59 A. V. Rayer, K. Z. Sumon, L. Jaffari and A. Henni, *J. Chem. Eng. Data*, 2014, **59**, 3805–3813.

60 A. Nonat, C. Gateau, P. H. Fries and M. Mazzanti, *Chem. – Eur. J.*, 2006, **12**, 7133–7150.

61 L. E. Kapinos and H. Sigel, *Inorg. Chim. Acta*, 2002, **337**, 131–142.

62 J. K. Romary, J. D. Barger and J. E. Bunds, *Inorg. Chem.*, 1968, **7**, 1142–1145.

63 A. Forgács, M. Regueiro-Figueroa, J. L. Barriada, D. Esteban-Gómez, A. de Blas, T. Rodríguez-Blas, M. Botta and C. Platas-Iglesias, *Inorg. Chem.*, 2015, **54**, 9576–9587.

64 L. Li, J. Rousseau, M. de, G. Jaraquemada-Peláez, X. Wang, A. Robertson, V. Radchenko, P. Schaffer, K.-S. Lin, F. Bénard and C. Orvig, *Bioconjugate Chem.*, 2021, **32**, 1348–1363.

65 R. Uzal-Varela, A. Rodríguez-Rodríguez, H. Wang, D. Esteban-Gómez, I. Brandariz, E. M. Gale, P. Caravan and C. Platas-Iglesias, *Coord. Chem. Rev.*, 2022, **467**, 214606.

66 L. Tei, Z. Baranyai, L. Gaino, A. Forgács, A. Vágner and M. Botta, *Dalton Trans.*, 2015, **44**, 5467–5478.

67 E. T. Clarke and A. E. Martell, *Inorg. Chim. Acta*, 1991, **190**, 37–46.

68 A. N. Carneiro Neto, R. T. J. Moura, L. D. Carlos, O. L. Malta, M. Sanadar, A. Melchior, E. Kraka, S. Ruggieri, M. Bettinelli and F. Piccinelli, *Inorg. Chem.*, 2022, **61**, 16333–16346.

69 T. Gallavardin, M. Maurin, S. Marotte, T. Simon, A.-M. Gabudean, Y. Bretonnière, M. Lindgren, F. Lerouge, P. L. Baldeck, O. Stéphan, Y. Leverrier, J. Marvel, S. Parola, O. Maury and C. Andraud, *Photochem. Photobiol. Sci.*, 2011, **10**, 1216–1225.

70 W. H. William and De. and D. R. Sudnick, *J. Am. Chem. Soc.*, 1979, **101**, 334–340.

71 W. DeW Horrocks, D. R. Sudnick, W. D. W. Horrocks and D. R. Sudnick, *Acc. Chem. Res.*, 1981, **14**, 384–392.

72 T. Kimura and Y. Kato, *J. Alloys Compd.*, 1998, **275–277**, 806–810.

73 K. Sénéchal-David, A. Hemeryck, N. Tancrez, L. Toupet, J. A. G. Williams, I. Ledoux, J. Zyss, A. Boucekkine, J.-P. Guégan, H. Le Bozec and O. Maury, *J. Am. Chem. Soc.*, 2006, **128**, 12243–12255.

74 A. D'Aléo, F. Pointillart, L. Ouahab, C. Andraud and O. Maury, *Coord. Chem. Rev.*, 2012, **256**, 1604–1620.

75 J.-C. G. Bünzli and S. V. Eliseeva, in *Lanthanide Luminescence: Photophysical, Analytical and Biological Aspects*, ed. P. Hanninen and H. Harma, Springer-Verlag Berlin Heidelberg, 2010, pp. 1–45.

76 K. Binnemans, *Coord. Chem. Rev.*, 2015, **295**, 1–45.

77 P. A. Tanner, *Chem. Soc. Rev.*, 2013, **42**, 5090–5101.

78 R. D. Peacock, *The intensities of lanthanide f ↔ f transitions BT - Rare Earths*, Springer Berlin Heidelberg, Berlin, Heidelberg, Heidelberg, 1975, vol. 22.

79 W. T. Carnall, P. R. Fields and K. Rajnak, *J. Chem. Phys.*, 1968, **49**, 4443–4446.

80 K. Lunstroot, P. Nockemann, K. Van Hecke, L. Van Meervelt, C. Görller-Walrand, K. Binnemans and K. Driesen, *Inorg. Chem.*, 2009, **48**, 3018–3026.

81 E. Kreidt, L. Arrico, F. Zinna, L. Di Bari and M. Seitz, *Chem. – Eur. J.*, 2018, **24**, 13556–13564.

82 G. Stein and E. Würzberg, *J. Chem. Phys.*, 1975, **62**, 208–213.

83 B. Doistau, J.-R. Jiménez and C. Piguet, *Front. Chem.*, 2020, **8**, 555.

84 J. D. Saxe, T. R. Faulkner and F. S. Richardson, *J. Chem. Phys.*, 1982, **76**, 1607–1623.

85 B.-A. N. Willis, D. Schnable, N. D. Schley and G. Ung, *J. Am. Chem. Soc.*, 2022, **144**, 22421–22425.

86 M. Deng, N. D. Schley and G. Ung, *Chem. Commun.*, 2020, **56**, 14813–14816.

87 L. Arrico, C. De Rosa, L. Di Bari, A. Melchior and F. Piccinelli, *Inorg. Chem.*, 2020, **59**, 5050–5062.

88 K. M. Ayers, N. D. Schley and G. Ung, *Inorg. Chem.*, 2020, **59**, 7657–7665.

89 J. L. Lunkley, D. Shirotani, K. Yamanari, S. Kaizaki and G. Muller, *J. Am. Chem. Soc.*, 2008, **130**, 13814–13815.

This journal is © The Royal Society of Chemistry 2023

J. Mater. Chem. C, 2023, **11**, 4188–4202 | **4201**

90 Y. B. Tan, Y. Okayasu, S. Katao, Y. Nishikawa, F. Asanoma, M. Yamada, J. Yuasa and T. Kawai, *J. Am. Chem. Soc.*, 2020, **142**, 17653–17661.

91 J. D. Fradgley, A. T. Frawley, R. Pal and D. Parker, *Phys. Chem. Chem. Phys.*, 2021, **23**, 11479–11487.

92 E. Cavalli, C. Nardon, O. G. Willis, F. Zinna, L. Di Bari, S. Mizzoni, S. Ruggieri, S. C. Gaglio, M. Perduca, C. Zaccone, A. Romeo and F. Piccinelli, *Chem. – Eur. J.*, 2022, **28**, e202200574.

93 H. Sund, Y.-Y. Liao, C. Andraud, A. Duperray, A. Grichine, B. Le Guennic, F. Riobé, H. Takalo and O. Maury, *Chem. Phys. Chem.*, 2018, **19**, 3318–3324.

94 A. T. Bui, M. Beyler, Y.-Y. Liao, A. Grichine, A. Duperray, J.-C. Mulatier, B. Le Guennic, C. Andraud, O. Maury and R. Tripier, *Inorg. Chem.*, 2016, **55**, 7020–7025.

95 A. Picot, A. D'Aléo, P. L. Baldeck, A. Grichine, A. Duperray, C. Andraud and O. Maury, *J. Am. Chem. Soc.*, 2008, **130**, 1532–1533.

96 K. Y. Zhang, Q. Yu, H. Wei, S. Liu, Q. Zhao and W. Huang, *Chem. Rev.*, 2018, **118**, 1770–1839.

97 E. Deiters, B. Song, A.-S. Chauvin, C. D. B. Vandevyver, F. Gumy and J.-C. G. Bünzli, *Chem. – Eur. J.*, 2009, **15**, 885–900.

98 J. Mendy, A. Thy Bui, A. Roux, J.-C. Mulatier, D. Curton, A. Duperray, A. Grichine, Y. Guyot, S. Brasselet, F. Riobé, C. Andraud, B. Le Guennic, V. Patinec, P. R. Tripier, M. Beyler and O. Maury, *ChemPhysChem*, 2020, **21**, 1036–1043.

99 C. Cottet-Rousselle, X. Ronot, X. Leverve and J.-F. Mayol, *Cytometry Part A*, 2011, **79A**, 405–425.

4202 | *J. Mater. Chem. C*, 2023, **11**, 4188–4202

This journal is © The Royal Society of Chemistry 2023